HHS Public Access

Author manuscript

Med Phys. Author manuscript; available in PMC 2025 January 01.

Published in final edited form as:

Med Phys. 2024 January ; 51(1): 494–508. doi:10.1002/mp.16726.

Evaluation of ion chamber response for applications in electron FLASH radiotherapy

Kevin Liu[a,b], **Shannon Holmes**[c], **Brian Hooten**[c], **Emil Schüler**[a,b,†,*], **Sam Beddar**[a,b,†,*]

[a]Division of Radiation Oncology, Department of Radiation Physics, The University of Texas MD Anderson Cancer Center, Houston, Texas, USA

[b]Graduate School of Biomedical Sciences, The University of Texas, Houston, Texas, USA

[c]Standard Imaging Inc., Middleton, WI, USA

Abstract

Background: Ion chambers are required for calibration and reference dosimetry applications in radiation therapy (RT). However, exposure of ion chambers in ultra-high dose rate (UHDR) conditions pertinent to FLASH-RT leads to severe saturation and ion recombination, which limits their performance and usability. The purpose of this study was to comprehensively evaluate a set of commonly used commercially available ion chambers in RT, all with different design characteristics, and use this information to produce a prototype ion chamber with improved performance in UHDR conditions as a first step toward ion chambers specific for FLASH-RT.

Methods: The Advanced Markus and Exradin A10, A26, and A20 ion chambers were evaluated. The chambers were placed in a water tank, at a depth of 2 cm, and exposed to an UHDR electron beam at different pulse repetition frequency (PRF), pulse width (PW), and pulse amplitude settings on an IntraOp Mobetron. Ion chamber responses were investigated for the various beam parameter settings to isolate their dependence on integrated dose, mean dose rate and instantaneous dose rate, dose-per-pulse (DPP), and their design features such as chamber type, bias voltage, and collection volume. Furthermore, a thin parallel-plate (TPP) prototype ion chamber with reduced collector plate separation and volume was constructed and equally evaluated as the other chambers.

Results: The charge collection efficiency of the investigated ion chambers decreased with increasing DPP, whereas the mean dose rate did not affect the response of the chambers (±1%). The dependence of the chamber response on DPP was found to be solely related to the total dose within the pulse, and not on mean dose rate, PW, or instantaneous dose rate within the ranges investigated. The polarity correction factor (P_{pol}) values of the TPP prototype, A10, and Advanced

[*]**Correspondence**: Sam Beddar, PhD, and Emil Schüler, PhD, Department of Radiation Physics, Division of Radiation Oncology, The University of Texas MD Anderson Cancer Center, 1515 Holcombe Blvd, Houston, TX 77030, USA. abeddar@mdanderson.org, eschueler@mdanderson.org.

[†]Both senior authors contributed equally

All authors were involved in the conceptualization, writing, editing, and figure visualization. KL took the lead in data acquisition and initial data analyses. ES and SB were jointly responsible for project oversight, administration, and funding acquisition. All authors have read and agreed to the published version of the manuscript.

CONFLICT OF INTEREST

Shannon Holmes and Brian Hooten are employees at Standard Imaging.

Markus chambers were found to be independent of DPP and dose rate (±2%), while the A20 and A26 chambers yielded significantly larger variations and dependencies under the same conditions.

Conclusions: Ion chamber performance evaluated under different irradiation conditions of an UHDR electron beam revealed a strong dependence on DPP and a negligible dependence on the mean and instantaneous dose rates. These results suggest that modifications to ion chambers design to improve their usability in UHDR beamlines should focus on minimizing DPP effects, with emphasis on optimizing the electric field strength, through the construction of smaller electrode separation and larger bias voltages. This was confirmed through the production and evaluation of a prototype ion chamber specifically designed with these characteristics.

1 | INTRODUCTION

The full potential of radiation therapy (RT) as a cancer therapy is limited by its toxicity to normal tissue structures, especially critical structures adjacent to the treatment site. Preclinical data have indicated that delivering radiation at dose rates of 40 Gy/s or higher over a period less than 200 ms, commonly referred to as ultra-high dose rate (UHDR) irradiation, has been shown to have the radiobiological advantage of selectively sparing normal tissue while maintaining a tumoricidal effect in *in vivo* preclinical models, which has been dubbed the FLASH effect.[1–5] Although the FLASH effect has been observed in many organ systems, the physical characteristics of the radiation beam such as dose per pulse (DPP), pulse repetition frequency (PRF), pulse width (PW), mean dose rate, and instantaneous dose rate needed to achieve and optimize the FLASH effect are still largely unknown[6,7]. Difficulties in measuring these irradiation parameters with conventional detectors and measurement techniques have led to underreporting and inconsistencies in the published literature. Available radiation detectors that are dose rate independent such as radiochromic film, thermoluminescence detectors, alanine, and methyl viologen[8,9] are not capable of real-time dose measurements or beam monitoring. Nevertheless, translation of FLASH-RT to the clinic is already underway, with one completed Phase I trial and at least two clinical trials currently recruiting in the United States and Europe,[10,11] despite these major limitations in the dosimetric evaluation and calibration of UHDR beamlines.

To elucidate the mechanism behind the FLASH effect, and to ensure accurate monitoring of the dose being delivered, accurate real-time radiation detectors that can operate within UHDR beamlines are urgently needed[12]. Currently, several studies have reported the use or the demonstration of real-time dosimeters capable of measuring the output of UHDR electron or proton beams in real-time such as diamond detectors, plastic scintillators, beam current transformers (BCTs), radioluminescent detectors, and Faraday cups[9,13–17]. Although they offer excellent temporal resolution (ns-μs range), these detectors are not perfect; they may suffer from a variety of dependencies in UHDR beamlines such as radiation damage, saturation, changes to sensitivity, energy dependence, and tissue non-equivalence. Traditionally, in the realm of RT, ionization (ion) chambers are used for the calibration of clinical linear accelerators under protocols established by the American Association of Physicists in Medicine (AAPM)[18–20] or the International Atomic Energy Agency (IAEA).[21,22] For this reason, ion chambers are regularly tested and calibrated at secondary standards laboratories to ensure accurate radiation dose measurements when used for clinical

or research applications.[23] However, the protocols recommended by the AAPM (TG-51)[18] or the IAEA (TRS-398)[22] cannot be applied directly to UHDR beamlines owing to the major saturation, ion recombination, and polarity effects induced in conventional ion chambers upon irradiation at dose rates and DPP values relevant to UHDR beamlines.[8,13] Standard models of characterizing ion chamber behavior such as Boag's two-voltage analysis[24] are also invalid under conditions of high-DPP and UHDR beamlines[8,13]. These limitations have downstream effects as well, since other detectors used to measure radiation are often cross-calibrated with ion chambers for accurate dose measurements. Therefore, there is a pressing need to evaluate existing chambers both to determine the current performance characteristics and to identify specific features of the ion chamber design that can be optimized in order to obtain more accurate readings in UHDR beamlines. The goal of this approach is to facilitate the clinical translation of FLASH-RT through the use of accepted AAPM protocols and to establish dose calibrations with detectors that are traceable to the National Institute of Standards and Technology (NIST).

Comprehensive evaluations of the dependencies of detectors in UHDR electron beamlines must consider the characteristics relevant to those beamlines, such as PW, DPP, mean and instantaneous dose rate, PRF, and total irradiation time[25]. Thus, radiation detectors must be characterized based on the isolated effects of these parameters. Unfortunately, such comprehensive evaluations are difficult to perform due to variability in machine performance when operating at these extreme dose rates and a lack of a "ground truth" to evaluate the detectors against. Currently, ion chambers evaluated for their response in UHDR electron beamlines include the PTW Advanced Markus chamber,[8,26] PTW Roos,[26,27] and a variety of custom-designed chambers such as end-window-chambers[28] with 0.5 to 2 mm electrode separation; ultra-thin parallel plate ion chambers[29] with 0.22 and 0.27 mm air gaps; and an ultra-thin parallel plate ionization chamber with a 0.25 mm air gap.[30] These reports have indicated through measurement or simulations that the charge collection efficiency, which includes the effects of saturation as well as ion recombination effects due to ion-ion and ion-electron recombination processes, depends strongly on DPP, and that modifications to ion chambers such as a higher bias voltage or a smaller electrode separation can improve charge collection efficiency and reduce the polarity effect exhibited by ion chambers in UHDR electron beamlines.

The work reported here represents one of the most comprehensive experimental evaluations of ion chambers in pulsed UHDR electron beamlines to date. This work involves experimental isolation of variable beam parameters, such as mean and instantaneous dose rate as well as DPP, that extends beyond what has been provided in previous studies, which either involve extensive simulations with limited experimental data to validate the findings or extensive experimental data without comprehensive isolation of each beam parameter. The ion chambers' response was evaluated against each individual beam parameter, including dose, DPP, mean dose rate, and instantaneous dose rate by modifying the number of pulses delivered, PW, PRF, and pulse amplitude[16]. The ion chambers' response was evaluated against dose rate independent BCTs, which represent the most accurate instrumentation available for real-time evaluation of UHDR electron beam parameters on a pulse-by-pulse basis[9,16,31]. The ion chambers' response was further evaluated as a function of ion chamber design, where the chambers included in this study represent a wide variety

of parallel plate chambers with different collecting volumes, collector plate separation, bias voltage capabilities, and materials, as well as a cylindrical micro chamber for reference. Based on this evaluation, a custom-designed thin parallel-plate (TPP) prototype ion chamber was developed to improve the ion chamber performance characteristics in UHDR electron beam conditions. This work addresses previous limitations in the methodology of detector performance evaluation in UHDR irradiation conditions and the results obtained on ion chamber response will help to shape future ion chamber designs for UHDR dosimetry applications.

2 | METHODS

The ion chambers evaluated in this study were the Advanced Markus (PTW, Freiburg, Germany), Exradin A10 Markus-type Chamber (Standard Imaging, Middleton, WI, USA), Exradin A26 Microchamber (Standard Imaging), Exradin A20 Low-Energy X-ray Chamber (Standard Imaging), and a TPP prototype ion chamber constructed based on the A20 ion chamber design but with a reduced electrode gap of 1 mm. Only one chamber of each model was tested. The goal of this study was to evaluate ion chambers with substantially different design characteristics from a wide array of ion chambers to inform future developments rather than evaluating subtle batch differences between ion chambers. The relevant specifications for each ion chamber are listed in Table 1. The specifications for the ion chambers came almost entirely from their respective vendor manual[32,33]. The average ion collection times for the ion chambers at their vendor specified maximum bias voltage, which was utilized in this study, were not listed in their vendor manual but were instead calculated using the equation: $\tau = \frac{d^2}{V \times k_i}$, where τ is the average ion collection time, d is the electrode spacing, V is the bias voltage (in this study we used the max bias voltage), and k_i is the ion mobility constant, specifically the positive ion mobility constant where k_i = 1.58 cm^2/Vs as calculated by Geleijns et al for positive ions[34]. In calculating the average ion collection time for the cylindrical ion chamber, we substituted the electrode spacing parameter (d) with the radius of cylindrical chamber (r = ½(Sensitive Volume Diameter – Collector Diameter)).

Before each irradiation session, the temperature and pressure were measured, recorded, and applied in corresponding correction factors to the measured signal.[18] The range of temperature and pressure values recorded over the entire time course of this experiment ranged from 294-296 K and 100.7-100.8 kPa. Each ion chamber investigated was connected to a SuperMAX electrometer (Standard Imaging) utilizing the maximum vendor-specified bias voltage, had a waterproof cap or sleeve placed on the chamber, and was inserted in a filled 1D Scanner (Sun Nuclear, Melbourne, FL, USA) water tank of dimensions 35 × 39 × 36.2 cm^3 for irradiations performed in both CONV and UHDR beamlines. To ascertain the chamber response at clinical dose rates and DPP values (i.e., 0.16 Gy/s and < 1mGy per pulse), the 16 MeV beam (R_{50} = 6.4 cm) on a Varian 21EX linear accelerator calibrated under the TG-51 protocol[18] was used under reference conditions with the chamber placed at a depth of maximum dose (d_{max}), 3.4 cm in water, such that it was situated in the flat region of the percent depth dose curve; 300 MU were delivered per measurement, and measurements were performed at bias voltages of −500 V and ±1000 V for the A10,

A20, A26, and TPP prototype ion chambers and −200 V and ±400 V for the Advanced Markus chamber. This procedure was done to calculate P_{ion} (the correction factor that accounts for ion recombination) and P_{pol} (the correction factor that accounts for the polarity effect in the chamber response)[18] at the vendor recommended maximum bias voltage for each ion chamber in a clinical beam (i.e., at conventional dose rates). Three consecutive measurements, corrected for temperature and pressure, were obtained for all ion chamber measurements used in this study unless specified otherwise.

$$P_{ion}(V_{max}) = \frac{1 - \frac{V_{max}}{V_{max/2}}}{\frac{M_{max}}{M_{max/2}} - \frac{V_{max}}{V_{max/2}}}, \quad (1)$$

$$P_{pol} = \left| \frac{M^{-}_{max} - M^{+}_{max}}{2M^{-}_{max}} \right|, \quad (2)$$

In equation 1, P_{ion} was calculated at the vendor recommended maximum bias voltage (V_{max}) and half-maximum bias voltage $V_{max/2}$ with their respective averaged measurements M_{max} and $M_{max/2}$ acquired at those voltages. In equation 2, P_{pol} was calculated at the vendor recommended maximum bias voltage (V_{max}) at both the negative and positive bias voltage with their respective averaged measurement, M^{-}_{max} and M^{+}_{max}, performed at those bias voltages.

The ion chamber evaluations in UHDR electron beamlines were performed using the Mobetron[35] (IntraOp, Sunnyvale, CA, USA). The Mobetron can deliver both UHDR and CONV dose rate beams with variable parameters such as beam energy, PW, number of pulses, PRF, and SSD.[35] BCTs (Bergoz Instrumentation, Saint-Genis-Pouilly, France) integrated into the head of the Mobetron were used to monitor and record the beam parameters of each individual pulse delivered in UHDR electron conditions[16]. The BCTs in this work represent the working standard against which the ion chambers were evaluated when placed in water. For dosimetric reporting, the BCTs were calibrated against energy- and dose rate-independent radiochromic film (Gafchromic EBT3, Ashland Inc., Covington, KY, USA) at each reference setup for the ion chambers placed in water as previously reported.[16,36] Except when explicitly noted, the settings used on the Mobetron were a 9 MeV UHDR beam (R_{50} = 4 cm) with a PRF of 90 Hz and the widest PW setting of 3.6 μs (corresponding to a DPP of 6.4 Gy), with the measurement setup directly below the exit window of the head of the Mobetron to achieve the highest DPP for the PWs available. The ion chamber response was evaluated in terms of the charge collection efficiency and P_{pol} as defined in TG-51[18] . The charge collection efficiency is defined as the percentage of the temperature and pressure corrected signal (M_{UHDR}) per unit dose (D_{UHDR}), measured using Gafchromic film and the BCTs, that is delivered to the ion chamber in an 9 MeV (R_{50} = 4 cm) UHDR beamline at a depth of 2 cm (d_{max}) divided by the fully corrected

signal (M_{CONV}) per unit dose (D_{CONV}), measured using Gafchromic film, delivered to the ion chamber in a 16 MeV (R_{50} = 6.4 cm) CONV beamline at a depth of 3.4 cm (d_{max}), as shown in Equation 3.[8] The depth of the measurements for the respective beam energies were selected based on their location in the flat part of the percent depth dose curve. The fully corrected signal includes correction factors involving P_{ion}, P_{pol}, P_{TP}, and P_{elec} (assumed equal to 1).[18]

$$Charge\ Collection\ Efficiency = \frac{M_{UHDR}/D_{UHDR}}{M_{CONV}/D_{CONV}} \times 100\% \quad (3)$$

When comparing the ion chamber response under different conditions of mean and instantaneous dose rate, a common metric used to evaluate their response was the coefficient of variation, which is the percent ratio of the standard deviation to the mean value of the dataset evaluated. In plotting the charge collection efficiency and P_{pol} as a function of various beam parameters related to dose, DPP, and dose rate, the error bars shown represent two standard deviations taken from three consecutive readings and may sometimes be hidden by the measurement points because of their relatively small values.

2.1 | Bias voltage response

To evaluate how each ion chamber's response at the highest PW (3.6 μs) and DPP (6.4 Gy) setting, in terms of charge collection efficiency (Eq. 3), was influenced by the applied bias voltage, the bias voltage was incrementally increased from 100 V to the vendor-recommended maximum bias voltage, which was 1000 V for all chambers investigated except for the Advanced Markus chamber, which has a maximum bias of 400 V (Table 1).

2.2 | Integrated Dose response

The response of the ion chambers as a function of dose was evaluated at the highest PW (3.6 μs) and DPP (6.4 Gy) setting. The accumulated signal from each chamber was recorded after the delivery of a set number of pulses ranging from 1 to 200 pulses (Table 1).

2.3 | Mean dose rate response

The ion chamber response in terms of charge collection efficiency and P_{pol} as a function of mean dose rate was evaluated at a DPP of 6.38 ± 0.29 Gy. The PRF settings examined ranged from 30 to 120 Hz, corresponding to mean dose rates ranging from 241 to 963 Gy/s. The mean dose rate was calculated using the following equation (Eq. 4), with the number of pulses labeled as N_p:

$$Mean\ Dose\ Rate = \frac{DPP \times N_p}{\frac{N_p - 1}{PRF} + PW \times 10^{-6}} [Gy/s]. \quad (4)$$

2.4 | Dose per pulse response

2.4.1 Variable Pulse Width Response—The dependence of each ion chamber's response on DPP was evaluated in two ways: (1) by changing the PW while keeping the instantaneous dose rate (amplitude of the pulse) constant and (2) by changing the instantaneous dose rate (amplitude of the pulse) while keeping the PW constant. In the first approach, the DPP was changed by modifying the PW between 0.5 and 3.6 μs at a constant SSD. Measurements were obtained at the highest DPP setting possible for each PW by placing the linac head directly at the water surface, resulting in DPP values of 1.06 ± 0.05 to 6.32 ± 0.27 Gy, respectively.

2.4.2 Variable Instantaneous Dose Rate Response—In the second approach, the PW setting was held constant at 3.6 μs, and the DPP was modified by changing the SSD while delivering a set number of pulses at each SSD location with the chambers placed at d_{max} (2 cm depth in water). The range of DPP values investigated for each chamber was 0.36 ± 0.01 to 6.41 ± 0.07 Gy.

2.5 | Instantaneous dose rate (Pulse Width) response at a constant dose per pulse

The instantaneous dose rate in this paper is defined as the DPP divided by the PW, which is measured at full width at half maximum of the pulse[16,37,38]. Because the pulses delivered are not perfectly square[16], the instantaneous dose rate is defined as the average dose rate over the width at 50% of max amplitude of the pulse. The ion chamber response as a function of PW and instantaneous dose rate was assessed by matching the DPP delivered to the chambers for different PWs. This was accomplished by modifying the SSD for each PW selected to ensure that the DPP measured at the location of the ion chamber remained constant regardless of the PW setting used. The DPP values selected allow at least two PW settings with matched DPP values, which were approximately 1, 2, and 3 Gy per pulse. For a DPP of 1 Gy, the PWs that could produce a DPP of approximately 1 Gy at the location of the ion chamber ranged from 0.5 to 3.6 μs. For a DPP of 2 Gy, the PWs that could produce a measured DPP of approximately 2 Gy at the ion chamber location ranged from 1.2 to 3.6 μs. For a DPP of 3 Gy, the range of PWs used was 3 to 3.6 μs. Table 3 summarizes the parameters that were changed in conjunction with the parameters that remained constant in this study.

3. RESULTS

Table 4 lists the P_{ion} and P_{pol} values of the ion chambers investigated in this study after irradiation with a 16 MeV electron beam delivered at a conventional dose rate of 0.16 Gy/s.

3.1 | Bias voltage response

The ion collection efficiency for all tested chambers increased with increased bias voltage (100, 300, 500, 800, and 1000 V for the A10, A26, A20, and TPP prototype; and 100, 200, 300, and 400 V for the Advanced Markus). Using a bias voltage of 1000 V was found to have a charge collection efficiency approximately twice that measured at the manufacturer-recommended bias voltage of 300 V for the A10, A20, and A26. The same response was found for the TPP prototype chamber. For the Advanced Markus, using a bias voltage of 400

V demonstrated a charge collection efficiency that was 20% higher than that measured at 300 V under the same DPP and dose rate conditions (Fig. 1).

3.2 Integrated Dose response

A linear relationship between the measured signal with the dose delivered at the maximum bias voltage setting was observed for all the ion chambers, with an $R^2 > 0.99$ (Figure 2A). Figure 2B shows the charge collection efficiency as a function of dose delivered for each of the ion chambers investigated. The coefficients of variation of the charge collection efficiency measured at different doses in the A10, Advanced Markus, A26, and TPP prototype ion chambers in Figure 2B were within 1% of one another, whereas the coefficient of variation for the charge collection efficiency measured at different doses for the A20 was determined to be 3.3%, all at a dose range of 6.40 ± 0.26 to 1215 ± 34 Gy using a PW of 3.6 μs.

3.3 | Mean dose rate response

The charge collection efficiency and P_{pol} values at the maximum bias voltage setting were found to be independent of PRFs ranging from 30-120 Hz (mean dose rate) (<1% coefficient of variation), with the exception of the A20 chamber (Figure 3) at a PW setting of 3.6 μs. The range of values for the measured charge collection efficiency for each of the ion chambers were 2.3-2.4% (A20), 25.4-25.7% (A10), 35.6-36.0% (A26), 36.8-37.0% (Adv. Markus), and 67.6-68.2% (TPP). The range of values for the measured P_{pol} for each of the ion chambers were 1.55-1.60 (A20), 1.084-1.086 (A10), 1.481-1.485 (A26), 0.993-0.998 (Adv. Markus), and 1.076-1.086 (TPP).

3.4 | Dose per pulse response

3.4.1 | Variable Pulse Width Response—Figure 4 shows the charge collection efficiency and P_{pol} values at the maximum bias voltage setting for the ion chambers investigated at DPP values ranging from 1.06 ± 0.05 to 6.32 ± 0.27 Gy with corresponding PWs ranging from 0.5 to 3.6 μs and constant PRF of 90 Hz, with a constant instantaneous dose rate of 2 MGy/s. The charge collection efficiency was shown to decrease with increased DPP from increasing PW at the same SSD. The charge collection efficiency decreased from 52% to 26% for the A10 chamber, 65% to 36% for the A26, 64% to 37% for the Advanced Markus, 6.3% to 2.4% for the A20, and 99% to 67% for the TPP prototype chamber, when increasing the DPP from 1.06 ± 0.05 to 6.32 ± 0.27 Gy. The measured P_{pol} ranges were 1.04-1.08 for the A10 chamber, 1.24–1.48 for the A26, 0.995–1.005 for the Advanced Markus, 1.46–1.57 for the A20, and 1.063–1.086 for the TPP prototype chamber. At the maximum allowed bias voltage, the range of P_{pol} values measured in a UHDR beam were comparable with the P_{pol} values measured with a conventional dose rate beam for the TPP prototype (1.058) and the Advanced Markus (1.001) listed in Table 4, but these values were substantially different than what was measured in a conventional dose rate beam for the A10 (1.005), A20 (1.006), and the A26 (1.018) chambers.

3.4.2 | Variable Instantaneous Dose Rate Response—The DPP dependence of the ion chamber response in terms of charge collection efficiency and P_{pol} at the maximum chamber bias voltage was investigated at DPP values ranging from 1.06 ± 0.05 to 6.32

± 0.27 Gy and instantaneous dose rates ranging from 0.1 to 2 MGy/s, respectively, at a single PW of 3.6 μs (Figure 5) and PRF of 90 Hz using different SSDs. The charge collection efficiency decreased with increased DPP and instantaneous dose rate for all chambers evaluated. The TPP prototype chamber, however, demonstrated a plateau in the charge collection efficiency (>99%) at DPPs of ≤1 Gy. The charge collection efficiency decreased from 71% to 28% for the A10 chamber, 86% to 35% for the A26, 13.0% to 2.5% for the A20, 86% to 38% for the Advanced Markus, and 100% to 65% for the TPP prototype chamber, when increasing the DPP from 0.36 ± 0.01 to 6.41 ± 0.07 Gy, respectively. The measured P_{pol} ranges were 1.029–1.051 for the A10 chamber, 1.07–1.45 for the A26, 0.991–1.004 for the Advanced Markus, 1.43–1.71 for the A20, and 1.06–1.09 for the TPP prototype chamber.

3.5 | Instantaneous dose rate (Pulse Width) response at a constant dose per pulse

For each of the ion chambers evaluated, the charge collection efficiency measured at a DPP of 1 Gy was found to have a coefficient of variation of 3% for PWs ranging from 0.5–3.6 μs; at a DPP of 2 Gy the coefficient of variation was also measured to be within 3% for PWs ranging from 1.2–3.6 μs; and at a DPP of 3 Gy the charge collection efficiency measurements were found to be within 2% for PWs of 3 and 3.6 μs. The associated instantaneous dose rates affiliated with the charge collection efficiency at each PW at a given DPP are listed in Table 2 and shown in Figure 6. At the maximum bias voltage for each chamber evaluated and a constant PRF setting of 90 Hz, the range of PWs investigated were 0.5-3.6 μs at a DPP of 1 Gy, 1.2-3.6 μs at a DPP of 2 Gy, and 3-3.6 μs at a DPP of 3 Gy.

The coefficient of variation of the P_{pol} values for different PWs measured at a constant DPP of 1, 2, and 3 Gy for each of the ion chambers were within 2.2%, 2.0%, and 1.8%, respectively, with the highest variance observed in the A20 ion chamber. When the A20 ion chamber was excluded from consideration, the coefficients of variation for the P_{pol} values measured in the ion chambers for different PWs at DPPs ranging from 1 to 3 Gy were within 1%. The associated instantaneous dose rates affiliated with P_{pol} at each PW at a given DPP are listed in Table 2 and shown in Figure 7.

4 | DISCUSSION

This is the first comprehensive evaluation of Standard Imaging’s ion chambers, which are uniquely capable of having a maximum usable polarizing voltage of up to 1000 V. Overall, our results demonstrate that the charge collection efficiency of the evaluated ion chambers were strongly affected by the DPP of the beam; we further found them to be independent of the mean dose rate (up to 963 Gy/s) and of the instantaneous dose rate (up to 2 MGy/s). All ion chambers evaluated showed a strong dependence on DPP, irrespective of mean dose rate. The chambers were also found to be independent of PW and instantaneous dose rate as shown by the nonsignificant variation in charge collection efficiency as a function of PW when the DPP was matched between PWs. Furthermore, our study has also demonstrated that the SuperMAX electrometer in its current configuration does not demonstrate saturation within the experimental conditions and ion chambers evaluated based on the integrated dose response study. However, this does not indicate that the electrometer is perfectly optimized

for UHDR beamlines. Although no obvious electrometer saturation behavior was observed during this study, saturation of the individual pulse signals may still be occurring in the electrometer. Further investigation of the impulse response of electrometers used for UHDR dosimetry is warranted but is outside the scope of the current investigation.

The mean dose rate independence observed for these chambers may be due to the ion collection time being much shorter (on the order of μs[27]) than the time between each subsequent pulse delivery for the mean dose rate response (1/PRF), which is on the order of ms (8.3 ms was the shortest used in our measurements, i.e., at a PRF of 120 Hz). The longest ion collection time of the chambers evaluated was on the order of 100 μs. This would allow a theoretical PRF of 10 kHz to be used without inducing mean dose rate effects in the chamber, which is a significantly higher PRF setting than any standard linear accelerator currently in use or proposed for FLASH-RT applications[2,36]. The observed instantaneous dose rate independence may be due to the ion collection time being longer than the pulse duration for the ion chambers investigated in this study. For chambers with smaller electrode design, the collection time may be on the order of magnitude of μs and may yield instantaneous dose rate effects, as reported in a simulated study by Gomez et al[29], since τ is proportional to d^2. However, a separate simulation study from Kranzer et al. 2022 reports instantaneous dose rate independence for sub-mm ion chamber designs suggesting that such phenomenon arises from a static state in the electric field that is achieved in the ion chamber above a certain PW for a given electrode spacing, which is governed by the time of the slowest charge carriers to traverse the distance between the electrodes[30]. The same simulation study reports a less than 0.15% change in charge collection efficiency for different instantaneous dose rates (simulated as high as 3 MGy/s)[30]. These simulation studies highlight the need for a comprehensive experimental evaluation investigating the PW dependence of ion chambers at different DPPs and instantaneous dose rates, especially for chambers where the ion collection time is on par or shorter than the pulse duration.

A limitation to our estimation of the ion collection time is the assumption for the k_i value selected and the assumption that k_i is identical for all the chambers investigated in this study. In this study, the positive ion mobility constant (k_1) was selected for k_i as it is representative of the slowest ion mobility constant of the two presented (the other being the negative ion mobility constant (k_2)) and that the negative bias voltage setting was selected on the electrometer to collect positive ions. It is important to note that different authors have reported different ion mobility values for the positive ion mobility constant (k_1 =1.34-1.89 cm^2/Vs) and negative ion mobility constant (k_2 =1.85-2.21 cm^2/Vs) based on different assumptions for the recombination coefficient used in their calculation[34,39–42] with even some studies finding that $k_1 = k_2$ when the ions are freshly formed.[40,43] The average ion collection time was used as an approximation for the drift of the charges in the sensitive volumes, particularly in CONV beamlines, which may be subjected to variations when encountering UHDR and high DPP beamlines.

The DPP dependence of ion chamber response for different prototype constructions and the Advanced Markus in UHDR beamlines has been reported elsewhere[8,27–29]. The mean and instantaneous dose rate independence has been reported by Petersson et al. for only the Advanced Markus under conditions that the DPP remains the same (based on conclusions

drawn from their data but not directly measured), but to date the specific beam parameter dependence of ion chambers has not been isolated and directly measured in a systematic approach[8]. No other work has experimentally shown that the response of the ion chamber (in terms of charge collection efficiency and polarity) is independent of both the mean dose rate (up to 936 Gy/s) and instantaneous dose rate (up to 2 MGy/s), thereby demonstrating that the strongest, if not the only, dependence that ion chambers have regarding the physical beam parameter setting is in the DPP.

Slight discrepancies in the response of ion chambers for the PW response evaluation may reflect slight variations in the dose delivered when matching different PWs to the same DPP, inherent uncertainties related to film and BCTs[16], or that pulses delivered from the IntraOp Mobetron are not an ideal square function[16,31]. Gafchromic EBT3 film was selected as the dosimeter against which we calibrated the machine output due to its extensive use in UHDR beamlines, its known dose rate independence up to 10^{12} Gy/s[14,44], and its reported overall uncertainty of <4% (k=2)[45]. To mitigate the uncertainties related to repeat use of Gafchromic film, BCTs were also utilized to verify and confirm the dose measured by Gafchromic film by calibrating the BCT output to dose measured on Gafchromic film specific to each reference geometry[16]. Due to their high-accuracy and prompt real-time monitoring of the output from UHDR electron beamlines on a pulse-by-pulse basis, the BCTs provided measurement precision that was comparable to if not better than other established dose rate-independent dosimeters used in UHDR dosimetry (<1-2%)[9,16,31,46]. Even though introducing two separate dosimeters as the standard to which we compare the ion chamber response introduces additional systematic errors and uncertainty, we are comparing the relative response of ion chambers under different beam parameters of an UHDR beamline and are normalizing the charge per unit dose delivered with that measured in a CONV beamline to minimize the impact of this uncertainty in our data.

The reduction in charge collection efficiency with higher DPP is mitigated by using an ion chamber with a smaller electrode spacing or a higher bias voltage, both of which yield a larger electric field strength in the chamber volume. Smaller electrode spacing would ensure that the ions travel shorter distances to the electrode while increasing the bias voltage at a given electrode spacing would increase the electric field strength and more efficiently separate the ion pairs and reduce recombination as shown in this study[8,27–29]. The commercially available A10, A26, and the A20 are able to operate at a bias voltage of up to 1000 V, which is several hundred volts higher than could be achieved in other ion chambers tested or simulated in UHDR beamlines[8,27–29]. However, due to their current designs, their electric field strengths are much smaller thus prompting the design and evaluation of a prototype ion chamber with reduced electrode spacing but with retained bias voltage capability compared to the other chambers tested (up to 1000 V). The electrode gap was set to 1 mm to match the Adv. Markus chamber, albeit with a different collecting volume (0.003 vs 0.02 cm^3 for the TPP prototype and Adv. Markus respectively). Based on this comparison, we could conclude that when considering ion chamber design characteristics, volume had minimal or no effect on the ion chamber performance, and that the electrode separation was the determining factor, which was evident in our data when matching the electric field strength between the two chambers.

In the design of our prototype ion chamber, we did not go below 1 mm for the electrode gap. As demonstrated in this work, an avenue to improve the charge collection efficiency at higher DPPs would be the construction of parallel plate ion chambers with sub-mm electrode spacings. Since the SuperMAX electrometer has the capability to provide bias voltages as high as 1000 V, sub-mm ion chamber design would allow the user to examine different electric field strengths suitable to minimizing charge recombination as an avenue to designing a chamber with minimal saturation and recombination effects. Others have reported on designs of prototype parallel plate ion chambers with sub-mm (≤ 1 mm) electrode spacing that have utilized or simulated higher electric field gradients (going as high as 1200 V/mm), and these yielded improved charge collection efficiencies at higher DPP values[29,30]. However, it is important to note that given the same electric field gradient, chambers with a smaller electrode spacing were reported to show improved charge collection efficiencies as a function of DPP, emphasizing the influence that electrode spacing has over bias voltage of the chamber design[30]. This is shown in comparing the charge collection efficiency at 1000 V/mm measured by the TPP with those measured by sub-mm prototype chambers produced in previous papers[29,30]. An important observation to note is that the ion collection time (τ is proportional to d^2/V) is directly related to the electrode spacing (d) and inversely related to the electric field strength (V/d) indicating that higher electric field strengths paired with smaller electrode spacings will yield smaller ion collection times. Such combinations in the ion chamber design may result in ion chambers with an instantaneous dose rate or PW dependence where ion collection times will be on par or faster compared to the delivered radiation pulse.

With respect to chamber design, among the commercially available chambers from Standard Imaging, the A26 microchamber had higher charge collection efficiency compared to the A10 or A20 parallel plate chamber at the same operating bias voltage despite having a substantially dissimilar design than the two parallel plate chambers. This may be due to the maximum distance (1.27 mm) traveled by the ion pairs in the A26 microchamber being smaller than that of the A10 and A20 (Table 1) thus yielding a larger electric field strength than the two aforementioned ion chambers. We have showed in this work that ion chambers designed with smaller electrode spacing yield substantial improvements in charge collection efficiency, as demonstrated by the performance of the Advanced Markus and the TPP prototype chamber compared with the commercially available A10 and A20 parallel plate chambers. For instance, the Advanced Markus chamber, operating at a bias voltage of 400 V, demonstrates comparable if not better charge collection efficiency than the commercially available A10, A20, and A26 ion chambers operating at a bias voltage of 1000 V. This is true even when the electric field strength of the A10 chamber (500 V/mm) exceeded that of the Advanced Markus (400 V/mm) thereby emphasizing that both electric field strength and chamber design have a crucial role in the charge collection efficiency. At the 1000 V setting, only the TPP prototype showed improved charge collection efficiency over the Advanced Markus chamber, with a > 99% charge collection efficiency in UHDR beamlines at a DPP of 1 Gy or less.

When comparing ion chambers with identical electrode spacing (such as the 1 mm spacing in the TPP prototype and the Advanced Markus), the charge collection efficiencies were found to be on par with one another at the same bias voltage of 300 V (32% vs 34%

charge collection efficiencies) at the examined PW and DPP. Slight discrepancies in the charge collection efficiencies between the Advanced Markus and the TPP prototype could be attributable to measurement uncertainties related to the use of film (regarding the effective point of measurement and the inherent dosimetric uncertainties) as well as dissimilarities in design such as the guard ring width, stem orientation, and collecting volume between the two chambers. Kranzer et al.[28] has shown that ion chambers of dissimilar design but similar electrode spacings manifest similar charge collection efficiencies at the same bias voltage. However, it is important to note that the measured values in P_{pol} from Kranzer et al.[28] were reported to be dissimilar, indicating that ion chamber performance for P_{pol} may be dependent on other aspects of chamber design beyond electrode spacing and may be dependent on a combination of electrode spacing, DPP, and bias voltage. This was also observed in the Advanced Markus and the TPP prototype in this work. Furthermore, the performance between the Advanced Markus and the TPP in CONV beamlines was found to be substantially different in that the Advanced Markus had a much lower P_{ion} and P_{pol} than the TPP as recorded in Table 4. The TPP was designed as a proof-of-concept ion chamber that could be easily modified to pinpoint the features of an ion chamber that can be adapted to improve their performance in UHDR electron beamlines. Specifically, the TPP was based upon the A20 parallel plate chamber design, which was originally intended for low energy kV x-ray dosimetry. Because of its intended use, the A20 was designed such that the stem is oriented parallel to the beam, whereas the other chambers tested had the stem oriented perpendicular to the beamline. The large P_{pol} in the TPP A20 design likely arises from additional voltage-independent polarity effects arising from the induced Compton current to the stem in addition to any voltage-dependent polarity effects, which may be dependent on the electric field strength, electrode spacing, and the large collector diameter relative to the volume.

Regarding P_{pol}, it is important to note that a limitation to this study involves potential variation in the measured P_{pol} values at the same DPP observed when changing the experimental setup (such as the SSD) of the Mobetron for different beam deliveries. This is because the P_{pol} measured in parallel plate chambers was found to be dependent on the electron beam energy, field size, and the amount of cable/stem irradiated depending on their orientation relative to the beamline, all of which are affected by varying SSD[47]. In light of this, we report that the measured P_{pol} values were strongly affected by the DPP of the beam for the A26 microchamber and A20 parallel plate chamber, with the P_{pol} values becoming incrementally larger at higher DPPs until its value plateaus, but the measured polarity correction factor values in the Advanced Markus, A10, and the TPP prototype showed less variation, with polarity values within ±2% of the mean P_{pol} value measured between 0.36 ± 0.01 to 6.41 ± 0.07 Gy per pulse.

The relatively larger polarity effect in microchambers has been reported elsewhere[48–50]; specifically Miller et al.[48], who reported that the voltage-dependent polarity effects of microchambers arose from the potential difference between the guard and collecting electrodes of the chamber resulting in distortion of the electric field lines within the collecting volume and thereby affecting the chamber response. This is confirmed in our findings in demonstrating the P_{pol} dependence measured in the A26 at larger DPPs. For cylindrical chambers, a nonhomogeneous electric field within the air cavity induces

significant voltage-dependent polarity effects since the liberated electrons will reach the positive electrode without forming negative ions, thereby yielding substantially different charge collection efficiencies at opposite bias voltages[43,51]. As such, when examining the charge collection efficiency for the A26 at the positive and negative bias voltages, it was found that its performance significantly improves when a positive bias voltage was applied to collect the generated negative charge, even matching that of the TPP when plotting the charge collection efficiency as a function of DPP. The large P_{pol} value for the A20, as well as its dependency and larger variation in its measurements as a function of PRF and PW for both P_{pol} and charge collection efficiency, may have arisen from its substantially larger electrode spacing and lower electric field strength (200 V/mm) than other ion chambers investigated, which would result in a greater temporal and spatial charge imbalance within the collecting volume and therefore greater electric field distortion that becomes more severe at higher DPP values[28,30].

In this study, only the P_{pol} values of the TPP prototype and the Advanced Markus were found to remain unchanged when comparing their measured values in an UHDR electron beamline compared to what was measured in a CONV beamline. This may be an effect of the electrode spacing given that both the TPP prototype and the Adv. Markus had the smallest electrode spacing of 1 mm out of the other parallel plate chambers examined. This was also observed by Kranzer et al., who investigated the measured current at different polarizing voltages for different ion chamber electrode spacings and found that larger electrode spacings yielded higher polarity effects[28]. Regardless, in this study only the Adv. Markus had a P_{pol} value that was within ±1% in an UHDR electron beamline, at a bias voltage of ±400 V; the other chambers had polarity values that far exceed that value. It is difficult to pinpoint the central cause of the P_{pol} differences in chamber response in an UHDR beamline versus in a CONV beamline, but it may be a combination of the construction material, electrode spacing, collector diameter, the guard ring width of the chamber design, and possibly an optimal ratio between these design parameters, which will be investigated in future work.

Conclusions

In this work, we evaluated the charge collection efficiency and polarity response of five distinct ion chambers exposed to an UHDR electron beam with DPP values and mean dose rates of up to 6.4 Gy and 963 Gy/s, respectively. We confirmed that the charge collection efficiency depends strongly on the DPP of the beam delivered and was independent of other beam parameters such as dose, mean dose rate, and instantaneous dose rate. Moreover, use of increased bias voltage beyond the standard 300 V greatly improved the charge collection efficiencies due to the increase in the electric field strength in the ion chambers. Despite dissimilar collecting volumes, ion chambers with identical electrode separation yielded similar performance in terms of charge collection efficiency, as demonstrated by the Advanced Markus and the TPP prototype at the same bias voltage and field strength. In acquiring P_{pol} measurements at the maximum bias voltage, P_{pol} was found to be strongly dependent on DPP only for the A20 and the A26 but remained relatively constant for the Advanced Markus, A10, and TPP prototype with the Advanced Markus chamber having a P_{pol} closest to unity in both UHDR and CONV conditions. In summary, our findings

pinpoint that DPP is the most significant feature of the physical beam parameters that needs to be considered for ion chamber design in UHDR beamlines within the range of parameters used in this work. This dependency can be mitigated through ion chamber construction with smaller electrode separation and larger bias voltage capabilities. Future work will consider the optimal electric field strength and electrode separation combination required in modified parallel plate chambers that would optimize their design and performance in UHDR beamline without compromising their accuracy or usability.

ACKNOWLEDGEMENTS

We thank Christine F. Wogan, MS, ELS, of MD Anderson's Division of Radiation Oncology, for editorial contributions to this article. Research reported in this publication was supported by the National Cancer Institute of the National Institutes of Health under Topic 434-75N91022C00039 - Phase I SBIR Contract, R01CA266673, and P30 CA016672, by the University Cancer Foundation via the Institutional Research Grant program at MD Anderson Cancer Center, and by UTHealth Innovation for Cancer Prevention Research Training Program Pre-doctoral Fellowship (Cancer Prevention and Research Institute of Texas grant #RP210042). The content is solely the responsibility of the authors and does not necessarily represent the official views of the National Institutes of Health nor of the Cancer Prevention and Research Institute of Texas.

References

1. Okoro CM, Schüler E, Taniguchi CM. The Therapeutic Potential of FLASH-RT for Pancreatic Cancer. Cancers. 2022;14(5).
2. Schuler E, Acharya M, Montay-Gruel P, Loo BW Jr., Vozenin MC, Maxim PG. Ultra-high dose rate electron beams and the FLASH effect: From preclinical evidence to a new radiotherapy paradigm. Med Phys. 2022;49(3):2082–2095. [PubMed: 34997969]
3. Wilson JD, Hammond EM, Higgins GS, Petersson K. Ultra-High Dose Rate (FLASH) Radiotherapy: Silver Bullet or Fool's Gold?. Front Oncol. 2019;9:1563. [PubMed: 32010633]
4. Friedl AA, Prise KM, Butterworth KT, Montay-Gruel P, Favaudon V. Radiobiology of the FLASH effect. Medical Physics. 2022;49(3):1993–2013. [PubMed: 34426981]
5. Favaudon V, Caplier L, Monceau V, et al. Ultrahigh dose-rate FLASH irradiation increases the differential response between normal and tumor tissue in mice. Sci Transl Med. 2014;6(245).
6. Bourhis J, Montay-Gruel P, Gonçalves Jorge P, et al. Clinical translation of FLASH radiotherapy: Why and how?. Radiother Oncol. 2019;139:11–17. [PubMed: 31253466]
7. Valdes Zayas A, Kumari N, Liu K, et al. Independent Reproduction of the FLASH Effect on the Gastrointestinal Tract: A Multi-Institutional Comparative Study. Cancers. 2023;15(7).
8. Petersson K, Jaccard M, Germond JF, et al. High dose-per-pulse electron beam dosimetry - A model to correct for the ion recombination in the Advanced Markus ionization chamber. Med Phys. 2017;44(3):1157–1167. [PubMed: 28094853]
9. Romano F, Bailat C, Jorge PG, Lerch MLF, Darafsheh A. Ultra-high dose rate dosimetry: Challenges and opportunities for FLASH radiation therapy. Med Phys. 2022;49(7):4912–4932. [PubMed: 35404484]
10. Wu Y NH, Breitkreutz DY, Mascia AE, Moeckli R, Bourhis J, Schüler E, Maxim PG, Loo BW Jr. Technological Basis for Clinical Trials in FLASH Radiation Therapy: A Review. Appl Rad Oncol. 2021;10(2):6–14.
11. Mascia AE, Daugherty EC, Zhang Y, et al. Proton FLASH Radiotherapy for the Treatment of Symptomatic Bone Metastases: The FAST-01 Nonrandomized Trial. JAMA Oncol. 2023;9(1):62–69. [PubMed: 36273324]
12. Zou W, Zhang R, Schueler E, et al. Framework for Quality Assurance of Ultra-High Dose Rate Clinical Trials Investigating FLASH Effects and Current Technology Gaps. Int J Radiat Oncol Biol Phys. 2023. doi: 10.1016/j.ijrobp.2023.04.018.
13. Ashraf MR, Rahman M, Zhang RX, et al. Dosimetry for FLASH Radiotherapy: A Review of Tools and the Role of Radioluminescence and Cherenkov Emission. Frontiers in Physics. 2020;8.

14. Karsch L, Beyreuther E, Burris-Mog T, et al. Dose rate dependence for different dosimeters and detectors: TLD, OSL, EBT films, and diamond detectors. Med Phys. 2012;39(5):2447–2455. [PubMed: 22559615]
15. Poirier Y, Xu J, Mossahebi S, Therriault-Proulx F, Sawant A. Technical note: Characterization and practical applications of a novel plastic scintillator for online dosimetry for an ultrahigh dose rate (FLASH). Med Phys. 2022;49(7):4682–4692. [PubMed: 35462420]
16. Liu K PA, Chopra N, Velasquez B, Li Z, Beddar S, Schüler E. Dual beam-current transformer design for monitoring and reporting of electron ultra-high dose rate (FLASH) beam parameters. Journal of Applied Clinical Medical Physics. 2023.
17. Darafsheh A, Hao Y, Zhao X, et al. Spread-out Bragg peak proton FLASH irradiation using a clinical synchrocyclotron: Proof of concept and ion chamber characterization. Med Phys. 2021;48(8):4472–4484. [PubMed: 34077590]
18. Almond PR, Biggs PJ, Coursey BM, et al. AAPM's TG-51 protocol for clinical reference dosimetry of high-energy photon and electron beams. Med Phys. 1999;26(9):1847–1870. [PubMed: 10505874]
19. Das IJ, Cheng CW, Watts RJ, et al. Accelerator beam data commissioning equipment and procedures: report of the TG-106 of the Therapy Physics Committee of the AAPM. Med Phys. 2008;35(9):4186–4215. [PubMed: 18841871]
20. McEwen M, DeWerd L, Ibbott G, et al. Addendum to the AAPM's TG-51 protocol for clinical reference dosimetry of high-energy photon beams. Med Phys. 2014;41(4):041501. [PubMed: 24694120]
21. Andreo P BD, Hohlfeld K, et al. Absorbed Dose Determination in External Beam Radiotherapy: An International Code of Practice for Dosimetry based on Standards of Absorbed Dose to Water. IAEA Technical Reports Series no 398 Vienna: International Atomic Energy Agency; 2000.
22. Andreo P BD, Hohlfeld K, Huq MS, Kanai T, Laitano F, Smyth V, Vynckier S. IAEA TRS-398–Absorbed dose determination in external beam radiotherapy: an international code of practice for dosimetry based on standards of absorbed dose to water. International Atomic Energy Agency. International Atomic Energy Agency. 2000;18:35–36.
23. Muir BR. Ion chamber absorbed dose calibration coefficients, N(D,w), measured at ADCLs: distribution analysis and stability. Med Phys. 2015;42(4):1546–1554. [PubMed: 25832045]
24. Boag JW, Hochhauser E, Balk OA. The effect of free-electron collection on the recombination correction to ionization measurements of pulsed radiation. Phys Med Biol. 1996;41(5):885–897. [PubMed: 8735255]
25. Esplen N, Mendonca MS, Bazalova-Carter M. Physics and biology of ultrahigh dose-rate (FLASH) radiotherapy: a topical review. Phys Med Biol. 2020;65(23):23TR03.
26. Di Martino F, Giannelli M, Traino AC, Lazzeri M. Ion recombination correction for very high dose-per-pulse high-energy electron beams. Med Phys. 2005;32(7):2204–2210.
27. McManus M, Romano F, Lee ND, et al. The challenge of ionisation chamber dosimetry in ultra-short pulsed high dose-rate Very High Energy Electron beams. Sci Rep. 2020;10(1):9089. [PubMed: 32493952]
28. Kranzer R, Poppinga D, Weidner J, et al. Ion collection efficiency of ionization chambers in ultra-high dose-per-pulse electron beams. Med Phys. 2021;48(2):819–830. [PubMed: 33251606]
29. Gomez F, Gonzalez-Castano DM, Fernandez NG, et al. Development of an ultra-thin parallel plate ionization chamber for dosimetry in FLASH radiotherapy. Med Phys. 2022;49(7):4705–4714. [PubMed: 35416306]
30. Kranzer R SA, Rodríguez FG, Weidner J, Paz-Martín J, Looe HK, Poppe B. . Charge collection efficiency, underlying recombination mechanisms, and the role of electrode distance of vented ionization chambers under ultra-high dose-per-pulse conditions. Physica Medica. 2022 Dec 1;104:10–17. [PubMed: 36356499]
31. Oesterle R, Gonçalves Jorge P, Grilj V, et al. Implementation and validation of a beam-current transformer on a medical pulsed electron beam LINAC for FLASH-RT beam monitoring. J Appl Clin Med Phys. 2021;22(11):165–171.
32. PTW-Freiburg. Detectors for Ionizing Radiation. 2022.
33. Imaging S. Exradin Detectors. 2018.

34. Geleijns J, Broerse JJ, Zweers D. General ion recombination for ionization chambers used under irradiation conditions relevant for diagnostic radiology. Med Phys. 1995;22(1):17–22. [PubMed: 7715564]
35. Moeckli R, Goncalves Jorge P, Grilj V, et al. Commissioning of an ultra-high dose rate pulsed electron beam medical LINAC for FLASH RT preclinical animal experiments and future clinical human protocols. Med Phys. 2021;48(6):3134–3142. [PubMed: 33866565]
36. Schuler E, Trovati S, King G, et al. Experimental Platform for Ultra-high Dose Rate FLASH Irradiation of Small Animals Using a Clinical Linear Accelerator. International Journal of Radiation Oncology Biology Physics. 2017;97(1):195–203. [PubMed: 27816362]
37. Institute of Electrical and Electronics Engineers., Radatz J, IEEE Computer Society. Standards Coordinating Committee. The IEEE standard dictionary of electrical and electronics terms. 6th ed. New York, N.Y.: Institute of Electrical and Electronics Engineers; 1997.
38. Compatibility E. Electromagnetic Compatibility (EMC)—Part 4-4: Testing and Measurement Techniques—Electrical Fast Transient/Burst Immunity Test. Burst Immunity Test. 2012.
39. Biggs PJ, Nogueira IP. Measurement of the collection efficiency of a large volume spherical ionization chamber in megavoltage therapy beams. Med Phys. 1999;26(10):2107–2112. [PubMed: 10535627]
40. HA E On the nature of the negative and positive ions in air, oxygen and nitrogen. Physical Review. 1922;20:117.
41. JR G Saturation characteristics of parallel-plate ionization chambers. Physics in Medicine & Biology. 1964 9:143.
42. Ritz VH, Attix FH. An ionization chamber for kilocurie source calibrations. Radiat Res. 1962;16:401–415. [PubMed: 14492530]
43. Boag JW WT. The saturation curve at high ionization intensity. British Journal of Applied Physics. 1952;3:222.
44. Bazalova-Carter M, Liu M, Palma B, et al. Comparison of film measurements and Monte Carlo simulations of dose delivered with very high-energy electron beams in a polystyrene phantom. Medical Physics. 2015;42(4):1606–1613. [PubMed: 25832051]
45. Jaccard M, Petersson K, Buchillier T, et al. High dose-per-pulse electron beam dosimetry: Usability and dose-rate independence of EBT3 Gafchromic films. Med Phys. 2017;44(2):725–735. [PubMed: 28019660]
46. Jaccard M, Durán MT, Petersson K, et al. High dose-per-pulse electron beam dosimetry: Commissioning of the Oriatron eRT6 prototype linear accelerator for preclinical use. Med Phys. 2018;45(2):863–874. [PubMed: 29206287]
47. Aget H RJ. Polarity effect for various ionization chambers with multiple irradiation conditions in electron beams. 1991;18:67–72.
48. Miller JR, Hooten BD, Micka JA, DeWerd LA. Polarity effects and apparent ion recombination in microionization chambers. Med Phys. 2016;43(5):2141. [PubMed: 27147326]
49. Le Roy M, de Carlan L, Delaunay F, et al. Assessment of small volume ionization chambers as reference dosimeters in high-energy photon beams. Phys Med Biol. 2011;56(17):5637–5650. [PubMed: 21828908]
50. McEwen MR. Measurement of ionization chamber absorbed dose k(Q) factors in megavoltage photon beams. Med Phys. 2010;37(5):2179–2193. [PubMed: 20527552]
51. Looe HK, Busing I, Tekin T, et al. The polarity effect of compact ionization chambers used for small field dosimetry. Med Phys. 2018;45(12):5608–5621. [PubMed: 30294821]

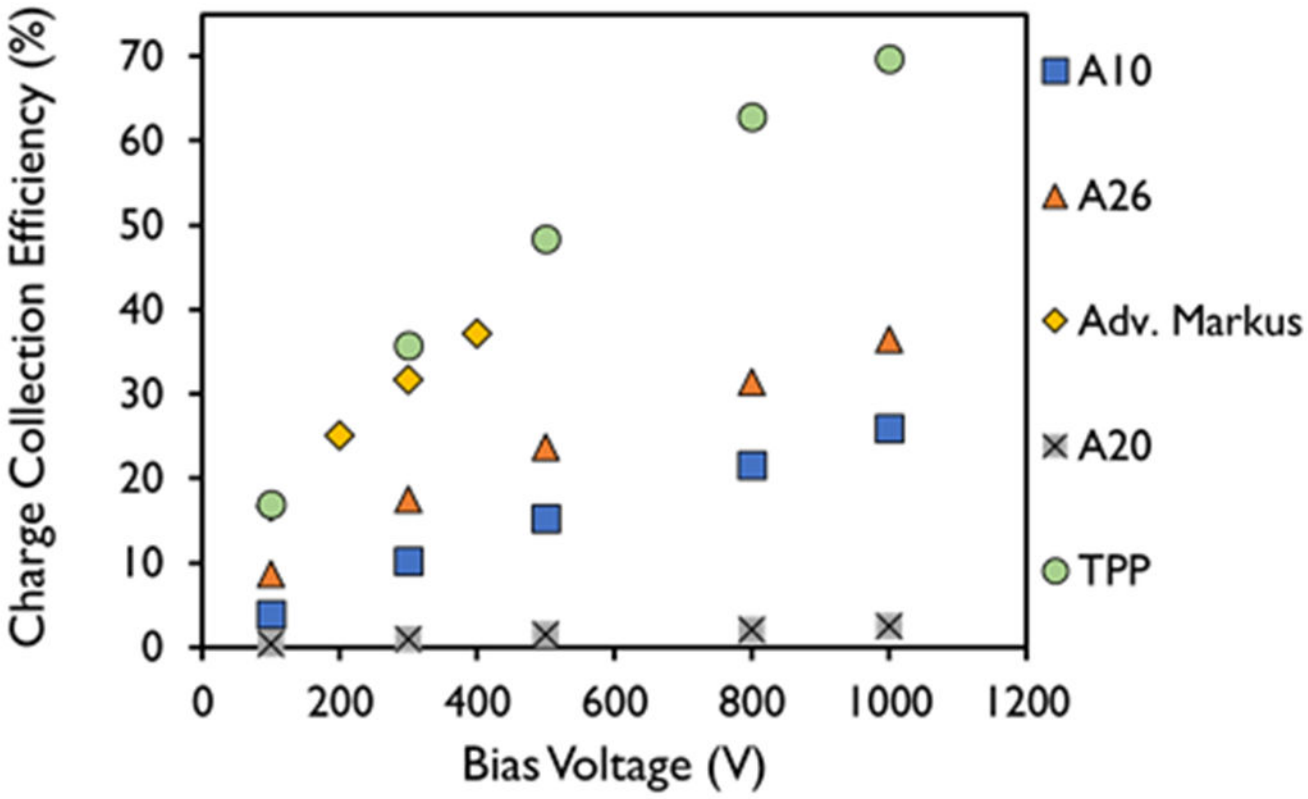

Figure 1.
Charge collection efficiency for different bias voltages measured in the A10, A26, Advanced Markus, A20, and thin parallel-plate (TPP) prototype ion chambers at a dose-per-pulse of 6.32 ± 0.27 Gy and a pulse width of 3.6 μs.

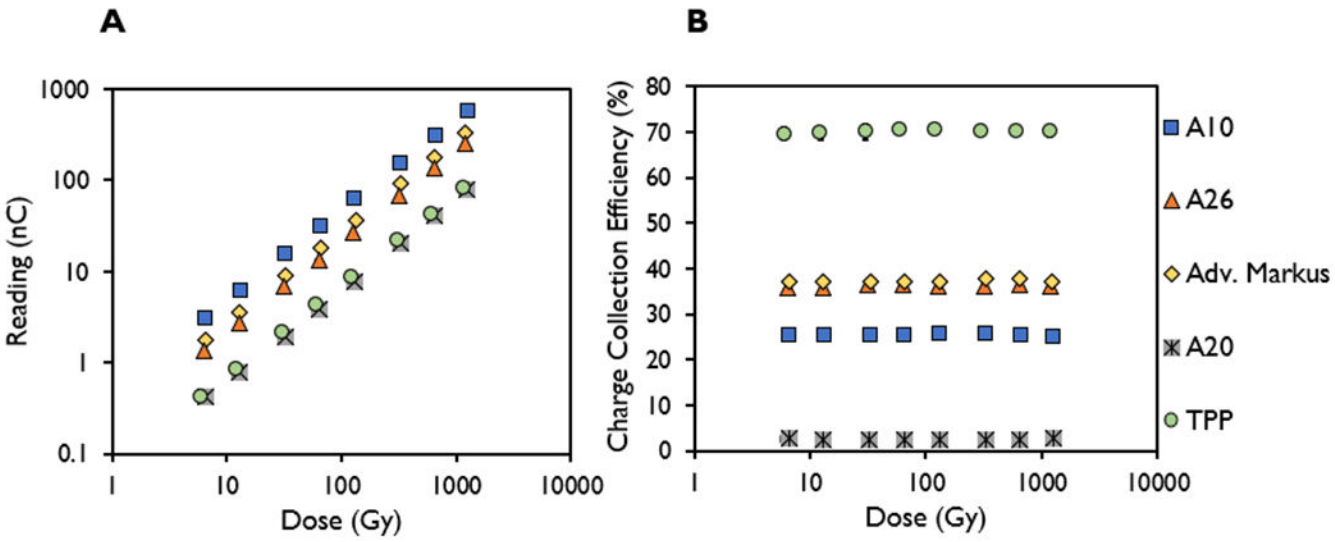

Figure 2.

Measured signal (nC) and charge collection efficiency (%) in the A10, A26, Advanced Markus, A20, and thin parallel-plate (TPP) prototype ion chambers plotted as a function of dose from the delivery of 1–200 pulses at pulse width of 3.6 μs and dose-per-pulse setting of 6.40 ± 0.26 Gy.

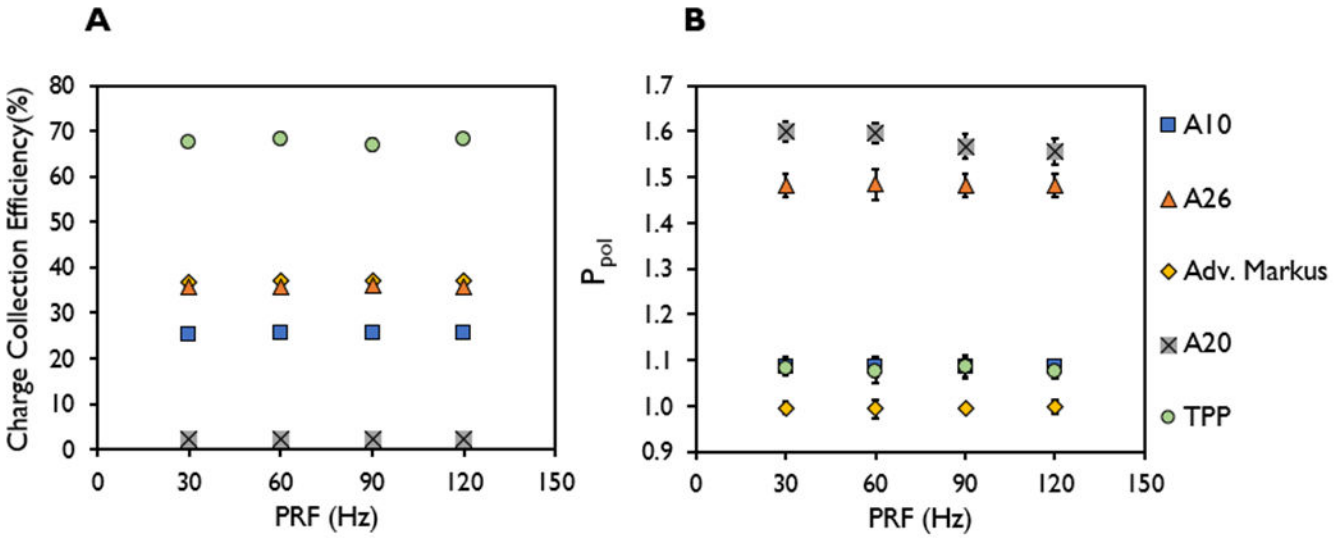

Figure 3.

(A) Charge collection efficiency and (B) polarity correction factor (P_{pol}) at pulse repetition frequencies of 30, 60, 90, and 120 Hz measured in the A10, A26, Advanced Markus, A20, and thin parallel-plate (TPP) prototype ion chambers at the highest dose-per-pulse (6.38 ± 0.29 Gy) at a pulse width of 3.6 μs.

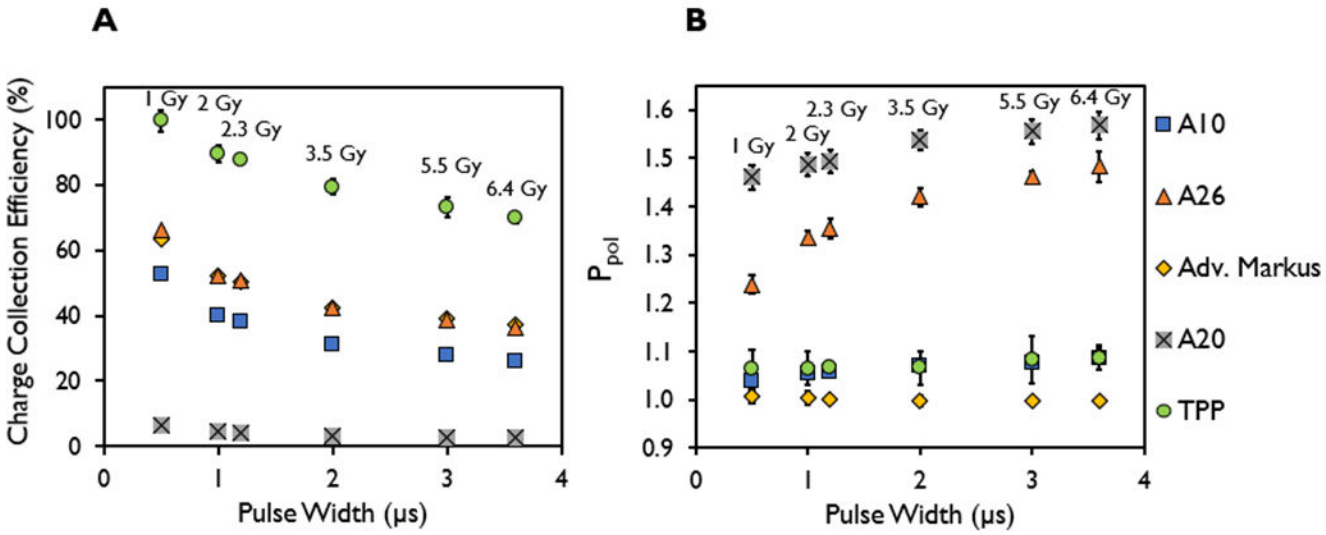

Figure 4.

(A) Charge collection efficiency and (B) polarity correction factor (P_{pol}) measured in the A10, A26, Advanced Markus, A20, and thin parallel-plate (TPP) prototype ion chambers at pulse widths of 0.5–3.6 μs and pulse repetition frequency of 90 Hz, with their corresponding dose-per-pulse for each pulse width (1.06 ± 0.05 to 6.32 ± 0.27 Gy).

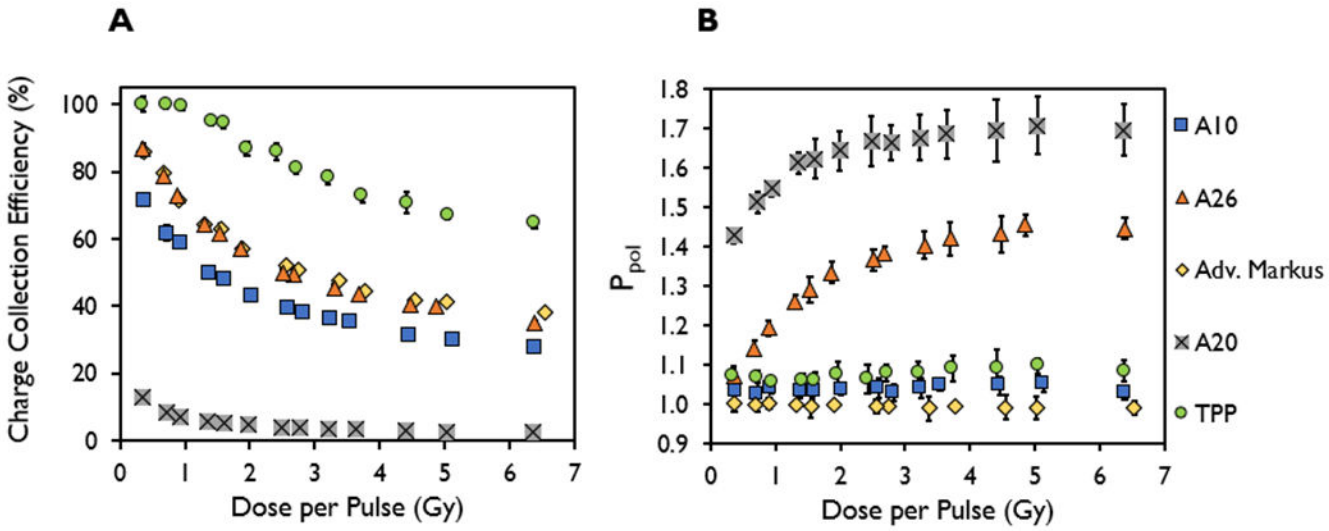

Figure 5.

(A) Charge collection efficiency and (B) polarity correction factor (P_{pol}) measured in the A10, A26, Advanced Markus, A20, and thin parallel-plate (TPP) prototype ion chambers at a constant pulse width of 3.6 μs and a pulse repetition frequency of 90 Hz, plotted as a function of dose-per-pulse ranging from 0.36 ± 0.01 to 6.41 ± 0.07 Gy.

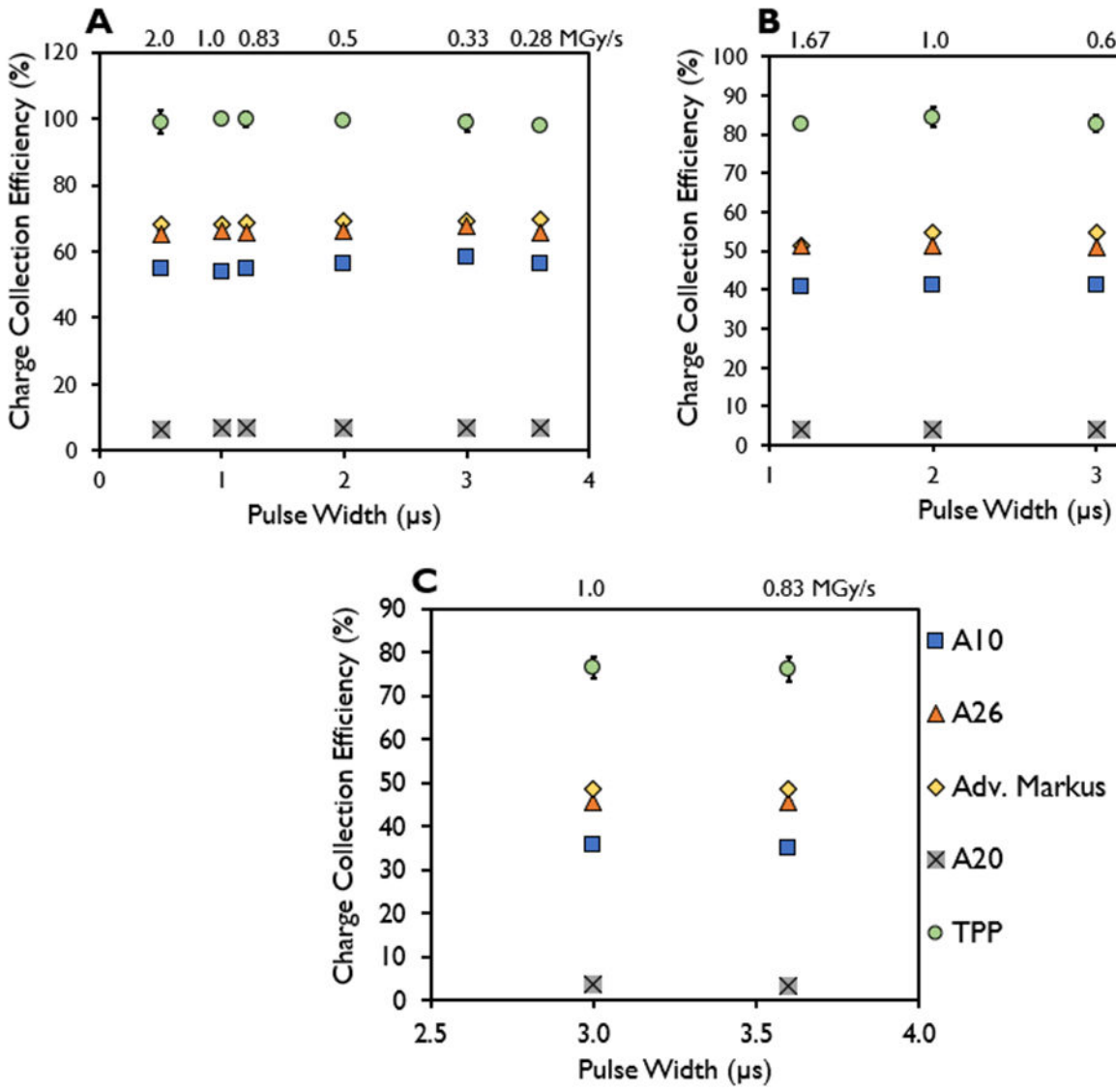

Figure 6.

Charge collection efficiency measured in the A10, A26, Advanced Markus, A20, and thin parallel-plate (TPP) prototype ion chambers at a constant dose-per-pulse of (A) 1 Gy, (B) 2 Gy, and (C) 3 Gy for the indicated pulse widths with the instantaneous dose rate included (MGy/s).

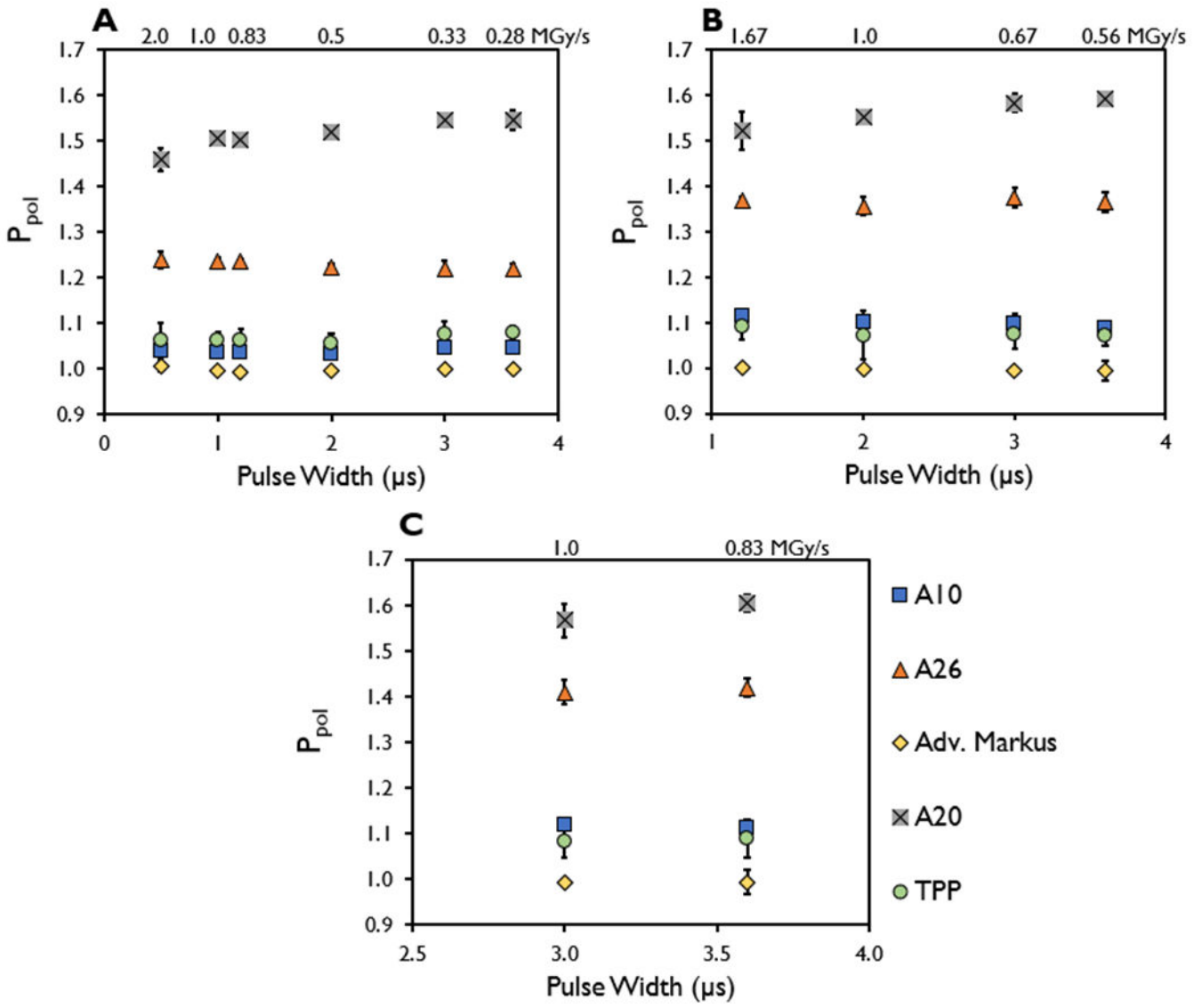

Figure 7.

Polarity correction factor (P_{pol}) measured in the A10, A26, Advanced Markus, A20, and TPP prototype ion chambers at a constant dose-per-pulse of approximately (A) 1 Gy, (B) 2 Gy, and (C) 3 Gy for the indicated pulse widths with the instantaneous dose rate included (MGy/s).

TABLE 1.

Ion chamber specifications

	Ion Chambers Tested				
	Adv. Markus	**A10**	**A20**	**A26**	**TPP prototype**
Chamber type	Parallel plate	Parallel plate	Parallel plate	Cylindrical	Parallel plate
Volume, [cm^3]	0.020	0.050	0.074	0.015	0.003
Maximum *and utilized bias voltage, [V]	400	1000	1000	1000	1000
Recommended *bias voltage, [V]	300	300	300	300	300
Utilized Electric Field Strength, [V/mm]	400	500	200	~787	1000
Collector gap, [mm]	1	2	5	NA	1
Collector diameter, [mm]	5	5.4	1.93	0.75	1.93
Guard ring width, [mm]	2	4.3	1.2	NA	1.2
Collecting Volume Outer Diameter [mm]	NA	NA	NA	3.3	NA
Average Ion Collection Time [μs] at maximum bias voltage	16	25	157	12	6.3

*The maximum and recommended bias voltages are vendor-specified values

TABLE 2.

Instantaneous dose-rate values, in kGy/s, for each pulse width, in μs, investigated and their corresponding doses per pulse, in Gy ranging from 278 kGy/s to 2 MGy/s

	Dose Per Pulse, Gy		
Pulse Width, μs	**1**	**2**	**3**
0.5	2000	NA	NA
1	1000	NA	NA
1.2	833	1667	NA
2	500	1000	NA
3	333	667	1000
3.6	278	556	833

Table 3.

Experiments in this study, with fixed and variable experimental parameters

Type of Study	Fixed (Unchanged) Parameters	Variable Parameters
Dose Linearity	Bias Voltage (Max V) Pulse Width (3.6 μs) Pulse Repetition Frequency (90 Hz) SSD Dose per Pulse (6.4 Gy)	Number of Pulses Delivered (Dose)
Pulse Width Dependence (Instantaneous Dose Rate)	Bias Voltage (± Max V) Pulse Repetition Frequency (90 Hz) Number of Pulses Delivered (5 pulses) Dose per Pulse (1-3 Gy)	Pulse Width (0.5-3.6 μs) SSD
Bias Voltage	Pulse Width (3.6 μs) Pulse Repetition Frequency (90 Hz) Number of Pulses Delivered (5 pulses) SSD Dose per Pulse (6.4 Gy)	Bias Voltage (100V – Max V)
Pulse Repetition Frequency (Mean Dose Rate)	Bias Voltage (± Max V) Pulse Width (3.6 μs) Number of Pulses Delivered (5 pulses) Dose per Pulse (6.4 Gy)	Pulse Repetition Frequency (30-120 Hz)
Dose Per Pulse (Constant SSD)	Bias Voltage (± Max V) Pulse Repetition Frequency (90 Hz) Number of Pulses Delivered (5 pulses) SSD	Pulse Width (0.5-3.6 μs) Dose per Pulse (1-6.4 Gy)
Dose per Pulse (Constant Pulse Width)	Bias Voltage (± Max V) Pulse Repetition Frequency (90 Hz) Number of Pulses Delivered (5 pulses) Pulse Width (3.6 μs)	SSD Dose per Pulse (0.3-6.4 Gy)

TABLE 4.

P_{ion} and P_{pol} values for the ion chambers measured and evaluated at the vendor recommended maximum bias voltage (Table 1) in a 16 MeV electron beam at a conventional dose rate (0.16 Gy/s)

	Ion Chambers Tested				
	Adv. Markus	**A10**	**A20**	**A26**	**TPP prototype**
P_{ion}	1.002	1.002	1.043	1.009	1.022
P_{pol}	1.001	1.005	1.006	1.018	1.058
Bias Voltage (V)	400	1000	1000	1000	1000